*Article*

# Analysis of building parameter uncertainty in district heating for optimal control of network flexibility

**Annelies Vandermeulen [1,2,4], Ina De Jaeger [1,3,4*], Tijs Van Oevelen [1,4], Dirk Saelens [1,3] and Lieve Helsen [1,2]**

1 EnergyVille; Thor Park 8310, 3600 Genk, Belgium
2 KU Leuven, Department of Mechanical Engineering; Celestijnenlaan 300, box 2421, 3001 Leuven, Belgium
3 KU Leuven, Department of Civil Engineering, Building Physics Section; Kasteelpark Arenberg 40, box 2447, 3001 Leuven, Belgium
4 VITO NV; Boeretang 200, 2400 Mol, Belgium
* Correspondence: ina.dejaeger@kuleuven.be

Version October 16, 2020 submitted to Energies

**Abstract:** Network flexibility is the use of the thermal capacity of water contained in the district heating network pipes to store energy and shift the heat load in time. Through optimal control, this network flexibility can aid in applications such as peak shaving and operational heat pump optimisation. Yet, optimal control requires perfect predictions and complete knowledge of the system characteristics. In reality, this is not the case and uncertainties exist. To get an insight in the importance of these uncertainties, this paper studies the influence of imperfect knowledge of building parameters on the optimal network flexibility activation and its performance. It is found that for the optimisation of heat pump operation, building parameter uncertainties do not present large risks. For peak shaving, a more robust result can be achieved by activating more network flexibility than may be required.

**Keywords:** district heating, optimal control, heat demand flexibility, building parameter uncertainty, robust control

## 1. Introduction

To limit air pollution and green house gas emissions, a fundamental change in our energy system is required. In 2019, heating and cooling in the tertiary and residential sectors were responsible for 41.7 % of the total final energy use in the EU28 [1], while 79 % of energy used in European households went to space heating (SH) and domestic hot water (DHW) [2]. Furthermore, 75 % of the energy used for heating and cooling of buildings is based on fossil fuels, while only 18 % originates from renewable and residual energy sources ($R^2ES$) (of which 90 % biomass) [3]. The heating and cooling sector for buildings thus represents a large fraction of the total energy use and is a viable opportunity to improve the system efficiency and the energy source portfolio.

Energy efficiency for the heating and cooling sector can be improved by district heating and cooling (DHC) systems in areas with a large heat/cold density, i.e. a large heat/cold demand per square kilometer. As Frederiksen and Werner stated, the fundamental idea of district heating (DH) is found in local synergies between heat sources and demand [4]. By connecting sources and demand through a pipe network, new heat and cold sources can be unlocked, such as combined heat and power (CHP), waste incineration, industrial residual heat, combustible renewables and geothermal sources, thereby improving energy efficiency and operational costs of the energy system. Connoly et al. [5] found that the inclusion of DHC in an EU energy efficiency strategy for 2050 can reduce the total costs for the heating and cooling of buildings by 15 %.

To increase the share of renewable and residual energy sources ($R^2ES$), their intermittency must be dealt with. One possible solution is to introduce energy flexibility in the energy system. Its definition is as follows [6]: '*Energy flexibility is the ability to shift the energy injection into or energy extraction from a system in time to bypass system limitations*.' By introducing energy flexibility, integration of $R^2ES$ can be improved by e.g. preventing curtailment. In this respect, DHC systems offer an interesting opportunity; they contain multiple thermal energy storage systems (TES), such as water storage tanks, aquifers, borefields, building thermal inertia, and the network itself. Intelligently deploying TES to create energy flexibility [7] can pave the way to large shares of $R^2ES$.

Within this context, this paper focuses on energy flexibility created by the thermal capacity of the water contained in DH network pipes, referred to as network flexibility from now on. By temporarily increasing/decreasing the supply temperature in the DH network, the network is charged/discharged. This way, energy can be stored for a while, bridging the gap between heat generation and heat demand. A detailed description of a typical network flexibility activation can be found in [6].

By solving an optimal control problem (OCP), two applications of network flexibility are considered in this paper. There is operational heat pump optimisation in which the interaction with the day-ahead market is optimised, and peak shaving in which the use of an expensive and/or polluting peak unit is minimised [8–10]. In the literature, other applications of network flexibility can be found: CHP optimisation [11–13], $R^2ES$ integration [14–16] and providing ancillary services [17].

However, the OCPs described in these studies all consider perfect predictions and perfect knowledge of the system model and parameters. However, this is not the case in reality and the OCP solution will deviate from the actual optimal control strategy. This study investigates the influence of these deviations on the control performance. Before going into the novelty and the specific research questions of this paper, the uncertainties that play a role in DH systems are introduced first, followed by a discussion on robust control of energy systems with uncertainty: how to determine a control strategy that can achieve a satisfactory result in (almost) all possible cases?

### 1.1. Uncertainties in district heating systems

Kim et al. [18] divided uncertainty into three categories. *Model uncertainties* are caused by a lack of knowledge regarding the physical system and/or the necessity to simplify and neglect certain aspects to keep the model solvable within acceptable time. *Process uncertainties* either refer to inaccurate actuators and sensors, or to the inability to measure certain system states. *Forecast uncertainties* relate to the imperfect forecasts made of system disturbances such as weather, electricity prices, $R^2ES$ generation, etc.

One example is heat demand uncertainty, which is in fact the result of other uncertainties. The main contributors are: user behaviour predictions, weather forecasts and unknown building construction. Of these, the former two are related to forecasts, while the latter belongs to the model uncertainties category.

To accommodate the user behaviour uncertainties, several tools have been set up to stochastically generate user behaviour profiles describing indoor temperature set-points, electrical appliance usage, internal heat gains and DHW use. These are mostly based on surveys and hence represent the typical behaviour of a certain population. Such tools include StROBe [19], Strathclyde University Demand Profile Generator [20], DELORES [21] and a Japanese activity-based modelling tool [22].

Regarding weather predictions, often weather servers that provide regular weather forecasts can be used to analyse weather uncertainties. For example, by combining imperfect weather forecasts with the corresponding measurements of the weather as it actually occurred, Oldewurtel [23] analysed the influence of these uncertainties for building heating.

The final contribution to heat demand uncertainty is the imperfect knowledge regarding building construction and building energy performance. Especially on district or city level, building energy performance related data is often unavailable [24,25]. Due to the lack of detailed input data on building level, archetype buildings are often used. Archetype buildings are buildings that are considered to be representative for a larger group of buildings. As an example, the TABULA project defines archetype dwellings, i.e. typical dwellings, for multiple European countries [26]. For Belgium, 30 archetype buildings are characterised in terms of their geometry and U-values for roof, ground floor, exterior wall and windows. Thanks to the rising popularity and availability of geographical information systems and geospatial data, the building geometry of all individual buildings can be included within district energy simulations. However, thermal quality data of the building envelope is still rarely available, although they are collected in some countries for the calculation and allocation of building energy performance certificates. Unfortunately, these data are often not shared due to privacy issues. To overcome this issue, De Jaeger et al. **[bijna gepubliceerde paper Ina]** developed a method to estimate the thermal quality of the building envelope based on construction year and geometrical data of the building based on statistical data from the Flemish energy performance certificates database.

In this paper, only the last source of heat demand uncertainty, the imperfect knowledge of building parameters, is discussed.

### *1.2. Robust control of energy systems*

With these uncertainties, the optimal solution of a deterministic OCP may be far from optimal for the actual system, leading to a reduced performance. Hence, OCPs have been reformulated in the literature to integrate uncertainties and to reduce the associated risk. Three approaches can be discerned, ranging in complexity.

Firstly, deterministic model predictive control (MPC) is a first step towards improved robustness. In short, an MPC solves an OCP with a receding horizon, i.e. at frequent points in time the OCP is solved with updated forecasts and system state measurements. The resulting optimal control strategy is then applied to the actual system [27]. Although the embedded OCP still does not consider the uncertainties, the regular update of relevant predictions and states ensures that the MPC control actions can adapt through time, all the while trying to minimise the objective. This technique is applied by Arnold and Göran [28] who alleviated prediction errors of electricity demand and $R^2$ES generation in an electricity system with connected TES systems. They analysed the MPC performance by running Monte-Carlo simulations and concluded that the TES systems provided the MPC with an opportunity to deal with most of the prediction errors, thereby preventing unplanned start-ups of plants.

A second approach uses stochastic modelling to determine the robust optimal control of a system. This is done by incorporating probability distributions for the stochastic parameters into the OCP. Different types of stochastic modelling can be found. In single-stage stochastic programming, all control actions are decided at one instance. This is e.g. the case in chance-constrained programming. Here, the chance that a certain constraint will be violated is limited to a certain extent. Bruninx et al. [29] applied such a chance constraint problem to ensure that the energy demand in an electricity system would be successfully generated and delivered in e.g. 95 % of the cases.

Two-stage optimisation problems are solved in two stages, as explained by Verrilli et al. [30]: *'In two-stage stochastic programs, the decision variables are divided into two groups: the first-stage variables, which have to be decided before the actual realisation of the uncertain parameters becomes available, and the second stage or recourse variables, which can be decided once the random events occur. These recourse variables are also interpreted as correction actions to compensate any infeasibility from the first-stage decisions.'* This technique has been applied multiple times. Wang et al. [31] applied it to the optimal control of a building energy system. To test the robust optimal control problem, they compared it to an MPC by running Monte-Carlo simulations of both controllers. They concluded the robust optimal control and the MPC reached about the same performance, but the stochastic OCP could do so with a single evaluation across the whole time horizon. Tian [17] optimised the operation of a CHP connected to both the electricity system and a DH system with a two-stage stochastic problem. The goal was to offer ancillary services and participate in the electricity spot market while the electricity demand is uncertain. Interestingly, network flexibility is applied here to increase the CHP profits, yet no DH system uncertainties were included.

Other stochastic programming techniques found in the literature include scenario robust optimisation, in which a number of carefully selected scenarios are combined [18] in one OCP. Options to select such scenarios include Sample Average Approximations [30], Monte-Carlo sampling [32], Latin Hypercube Sampling [18] and the point-estimate strategy [33,34]. Monte-Carlo least squares regression analysis [35] and min-max optimisations (worst-case optimisations) have also been applied for robust control of energy systems [36,37].

Finally, a third approach to reach robust control is by combining the first two: MPC and stochastic optimal control. While Oldewurtel [23] integrated a chance-constrained program for building energy system control into an MPC, Rantzer [38] and Verrilli et al. [30] both developed an MPC containing a two-stage optimisation problem for DH system control.

This overview shows that plenty of research in robust control of energy systems has been done. However, to the authors' knowledge, there has been no research yet in robust control of network flexibility with respect to heat demand uncertainty or any other form of uncertainty in the DH system itself. Hence, the exploratory study presented in this paper focusing only on the impact of building parameter uncertainty provides a valuable contribution to the scientific literature.

### *1.3. Novelty and research questions*

The main novelty of this paper is the assessment of building parameter uncertainties, leading to an uncertainty in the heat demand magnitude[1], impacting the network flexibility activation in DH systems based on a deterministic OCP. Two applications of network flexibility are studied: 1) operational heat pump optimisation in which the interaction of a central DH heat pump with the day-ahead electricity market is studied, 2) peak shaving.

This study indicates how sensitive the optimal network flexibility activation is to the building parameter uncertainties and hence a change in heat demand magnitude, and how much risk is associated with adopting a control strategy based on wrongly estimated building parameters. This paper shows whether simple measures can provide less risk and/or higher profits leading to a more robust control strategy. It is a first step in estimating the importance of robust network flexibility control and to the development of that robust control. The following research questions will be considered:

1. How does the optimal network flexibility activation (i.e. the control strategy) alter when the building parameters are different?
2. How sensitive is the network flexibility performance to the applied control strategy (and hence to uncertainty)?
3. Does this preliminary study lead to insights for a more robust activation of network flexibility?

In this paper, the considered case study is described first. Then, in Section 3, the methodology for the optimal control, the uncertainty on the heat demand and the uncertainty analysis is introduced. Subsequently, the results are presented in Section 4, followed by the discussion in Section 5. Finally, the conclusions are formulated in Section 6.

## 2. Case study: *GenkNET*

The influence of building parameter uncertainty on network flexibility is tested by optimising the control of *GenkNET*. This is a fictive DH system based on the city of Genk, Belgium. To set up this case study, steps 1-4 in Figure 1 were followed. First, the geometrical data from 7775 buildings located in Genk were collected from a CityGML LOD2 model. Then, Genk was divided into 9 neighbourhoods and for every neighbourhood the average construction year was determined by a *Google Streetview* scan. To determine the user behaviour of the people inhabiting these buildings, user behaviour profiles

---

[1] Uncertainty on the heat demand magnitude refers to a heat demand profile that has been scaled up/down with an uncertain (time-variable) factor. The 'magnitude' term is used in this text to emphasise that there are no timing changes. For an example of heat demand profiles that only have magnitude changes, please refer to Figure 5.

(temperature set-points, internal heat gains, DHW use, etc.) were generated with the stochastic toolbox StROBe [19].

**GenkNET DATA COLLECTION**

1. Collect geometry from CityGML LOD2 model for all buildings
2. Divide Genk into 9 residential neighbourhoods connected to the DH system
3. Estimate average construction year per neighbourhood
4. Allocate stochastic occupant behaviour based on StROBe

| OPTIMISE NEIGHBOURHOOD HEAT DEMAND PROFILES | CALCULATE UNCERTAINTY ON HEAT DEMAND PROFILES |
|---|---|
| 5. Allocate building envelope parameters based on TABULA | 9. Calculate 1 archetype per neighbourhood |
| 6. Allocate stochastic occupant behaviour based on StROBe | 10. Determine realistic input distributions for building envelope parameters per archetype based on probabilistic method |
| 7. Optimise heat demand per building using `modesto` | 11. Sample building envelope parameters for 500 variants per archetype |
| 8. Sum heat demand profiles for all buildings in neighbourhood | 12. Simulate heat demand of each variant using IDEAS |
| | 13. Calculate CV(Q) per archetype based on LDC |

14. Create 100 variants of heat demand profiles (step 8) using CV(Q) (step 13) per neighbourhood
15. Create 100 variants of GenkNET heat demand profiles by random selection of each neighbourhood

**Figure 1.** A flow chart describing the different steps taken to determine the *GenkNET* heat demand profiles including uncertainties (relevant to both Sections 2 and 3).

To limit the computational complexity of this case study and to prevent the simultaneous simulation of 7775 buildings, a thorough aggregation was carried out. Every neighbourhood in *GenkNET* is now represented by one substation that has to deliver the heat demand of the entire neighbourhood, neglecting the distribution network in a neighbourhood. For more details on this aggregation, please refer to [6]. This leads to the DH system layout shown in Figure 2. The nominal supply and return temperatures in this DH system are taken to be 57 °C and 37 °C, respectively. The pipe sizes are determined by the sizing procedure presented in [6].

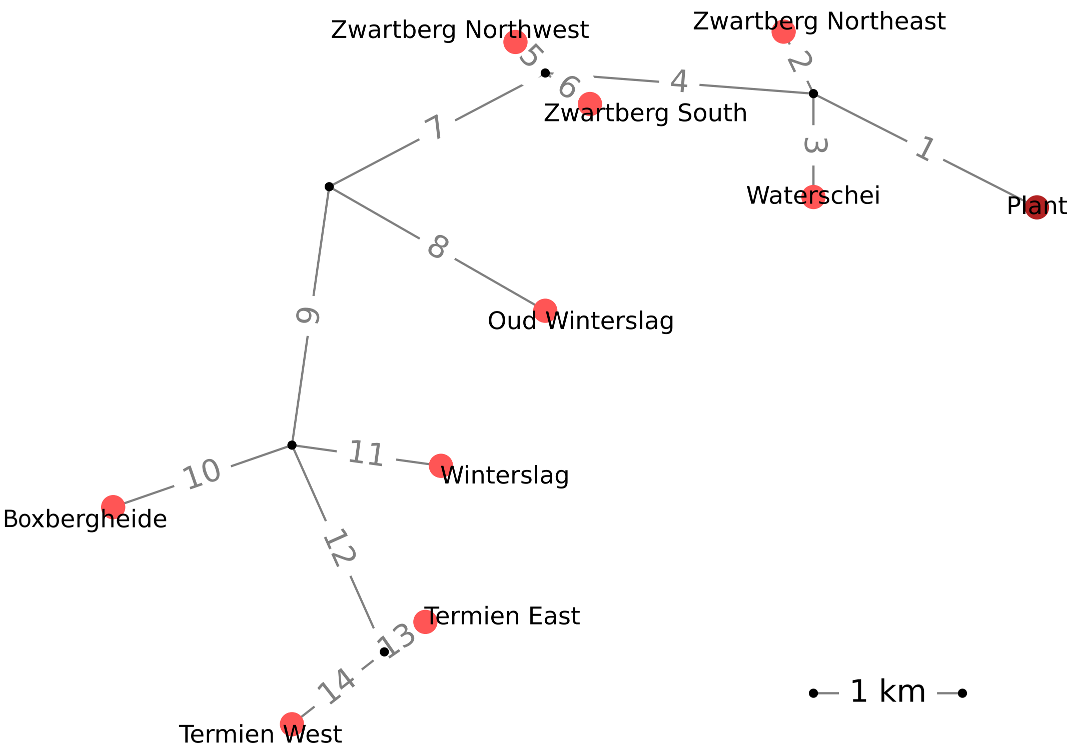


**Figure 2.** The lay-out of the aggregated *GenkNET*, indicating the position of the 9 neighbourhoods. There is a single heat generation site in the north-east of the network. The network pipes are indicated by the numbered lines.

Instead of a whole year analysis, only a limited number of days is tested in this paper. To select a representative set of days, two aspects are considered: 1) the overall heat demand, leading to a distinction between winter and transitional (spring and autumn) days. The summer days are not considered, as summer heat demands proved to be too low for interesting network flexibility activations and hence interesting results. 2) The day-ahead electricity price profile can be either stable and positive (small $\Delta p_e$), volatile and positive (large $\Delta p_e$), or become negative during the day (negative $p_e$). The electricity price $p_e$ corresponds to the BELPEX day-ahead market prices in 2014. This leads to a selection of 6 days, given in Table 1. These days will be referred to as <season>_<electricity price>, according to the names of the columns and rows of Table 1.

**Table 1.** The nine days selected for the *GenkNET* case. These days will be referred to as <season>_<electricity price>.

| **Heat demand** **El. price** | Winter | Trans(itional) |
|---|---|---|
| Small $\Delta p_e$ | 16/01 | 29/03 |
| Large $\Delta p_e$ | 14/01 | 17/11 |
| Neg(ative) $p_e$ | 16/02 | 16/03 |

In this paper, the heat generation unit is either a central air-to-water heat pump or a base/peak plant combination. The six selected days account for different electricity price profiles which allow to study different heat pump cases, as the operational heat pump optimisation heavily depends on the electricity price variation through time. To study the base/peak plant combination in more depth, different base load ratios are studied. The base load ratio $r_b$ defines the capacity of the base unit $\dot{Q}_{b,\,max}$ relative to the peak heat demand of the analysed day $\dot{Q}_{dem,max,\,day}$. Three base load ratios are tested: 60, 80 and 95 %. Note that this will lead to base plant sizes that are different for every case (day and base load ratio).

$$r_b = \frac{\dot{Q}_{b,\,max}}{\dot{Q}_{dem,max,\,day}} \tag{1}$$

## 3. Methodology

This section presents the methodology used. Firstly, it discusses the optimal control problems that will be solved in this study. Secondly, the set-up of the heat demand profiles with uncertainty is presented. Finally, the methodology of the uncertainty analysis to assess the influence of the building parameter uncertainty on network flexibility is described.

### *3.1. Deterministic optimal control*

To determine the optimal network flexibility activation, the toolbox `modesto` [39] is used. It contains a library of (non-linear) DH component models, including pipe, substation and heat generation models. The models as they are used in this study are presented in Appendix A. These models were developed specifically for determining optimal network flexibility activations. Hence, these models are suited to model the temporary network temperature changes in the DH network and the corresponding energy storage that take place during a network flexibility activation. For more information on the interactions that take place during a network flexibility activation, we refer to [6]. However, note that the models are completely deterministic and do not take into account any uncertainties.

`modesto` can automatically assemble the *GenkNET* DH system optimisation model based on its topology and a selection of models and optimisation objective. For each considered case, the network topology remains the same, yet the heat generation site and optimisation objective is changed depending on the studied case. In case of heat pump or peak shaving optimisation, either a heat pump model or a base/peak plant model is included. The optimisation objective depends on the heat generation site, Equations 2 and 3 show the objectives $C_{\mathrm{HP}}$ and $C_{\mathrm{PS}}$ for the operational heat pump and peak shaving optimisation, respectively. In these objectives, $\dot{W}$ is the electrical work done by the heat pump to generate the heat, $p_{\mathrm{e}}(i)$ is the day-ahead electricity market price during time step $i$, expressed in €/kWh$_{\mathrm{el}}$, $\Delta t$ is the time step between two points in time in the discretised OCP with a total of $N$ time steps. $\dot{Q}_{\mathrm{b}}$ and $\dot{Q}_{\mathrm{p}}$ are the heat delivered by the base and peak plant unit, respectively. Similarly, $p_{\mathrm{b}}$ and $p_{\mathrm{p}}$ are the prices of the heat generated by both units. They are expressed in €/kWh$_{\mathrm{th}}$ and are constant in time. This price already includes the plant energy efficiency. In this study, only the ratio between the two prices is imposed, equal to $p_{\mathrm{p}}/p_{\mathrm{b}} = 2$ [40].

$$C_{\mathrm{HP}} = \sum_{\mathrm{i}=1}^{N} p_{\mathrm{e}}(i)\dot{W}_{\mathrm{i}}\Delta t \tag{2}$$

$$C_{\mathrm{PS}} = \sum_{\mathrm{i}=1}^{N} (p_{\mathrm{b}}\dot{Q}_{\mathrm{b,i}} + p_{\mathrm{p}}\dot{Q}_{\mathrm{p,i}})\Delta t \tag{3}$$

The price of heat generation by the base unit is lower than that by a peak unit. Hence, the peak shaving objective causes a preference for the base unit and incentivises peak shaving. The heat pump objective incentivises heat generation on moments during which the electricity price is low. In this study, network flexibility is the only available tool in the OCP to create energy flexibility. By running the optimisation twice, once with network flexibility available, i.e. the supply temperature may change between its nominal value and a value that is 10 °C higher, and once with no network flexibility available, i.e. the supply temperature leaving the plant must remain equal to the nominal value, the network flexibility activation can be isolated. A more elaborate explanation on this workflow can be found in [41].

The OCP settings and models are elaborated on in Appendix A.

### *3.2. Heat demand profiles*

Following the process in Figure 1 (steps 5-15), heat demand profiles containing building parameter uncertainties can be set up.

In a first part (steps 5-8), the heat demand profile for every neighbourhood in *GenkNET* is determined based on a minimum energy use optimisation. Starting from the geometries of the 7775 buildings in Genk (step 1) and the neighbourhood construction year (step 3), building parameters are allocated to each building based on the TABULA archetype U-values [26]. Based on this data and the StROBe user behaviour profiles (step 4), van der Heijde calculated the building heat demand profiles [42], based on the 4$^{\mathrm{th}}$ order `TEASER` RC-model [43]. For this he used the typical meteorological year of Uccle, Belgium. To calculate the heat demand profiles, van der Heijde made use of `modesto` to determine the heat demand profile that ensures thermal comfort with minimum energy use in every building. Finally, to reach one heat demand profile per aggregated *GenkNET* neighbourhood, the heat demand profiles of buildings belonging to one neighbourhood are summed.

In a second part (steps 9-13), the uncertainty on the heat demand profiles is calculated. To reduce the computational burden, the uncertainty in each neighbourhood is determined through the use of archetype buildings. The archetype building for a neighbourhood is characterised by the estimated average construction year of the neighbourhood (step 3) and the average building geometry. To obtain the average building geometry, the geometry of all buildings is required (step 2). The areas of the façades and roofs are merged towards 4 orientations (N, E, S, W), with a negligible loss of accuracy [44]. This simplifies calculating the average. This procedure is repeated for every neighbourhood and results in nine archetype buildings.

For these nine archetype buildings, distributions on the U-values of the roof, ground floor, exterior wall and windows are introduced along with variations on the window-to-wall ratio, based on the method of De Jaeger et al. [**toekomstige paper Ina**]. These distributions are estimated to be as realistic as possible considering the scarcely available data of Genk [**toekomstige paper Ina**]. Note that building geometry is assumed to be known perfectly, as are user behaviour and weather predictions.

Using these distributions, 500 versions of every archetype building are generated. The distributions of all (9x500) generated building parameters can be seen in Figure 3. Next, yearlong simulations of the archetype buildings are carried out in Modelica using the IDEAS model library [45]. These simulations entail a 2-zone white-box model of the SH system consisting of ideal radiator heating. The user behaviour and weather as they were described in Section 2 are applied. This leads to the distribution in annual SH heat demand in *GenkNET* shown in Figure 4.

Based on the simulation results, load duration curves (LDC) of every variation are set up. The coefficient of variation[2] (CV) for one archetype was found to change in function of the expected SH heat demand of that building $\dot{Q}_{\text{arch, SH},\mu}$. Furthermore, the CV could be well estimated by an exponential in function of the expected SH heat demand of the archetype building, with $a$, $b$ and $c$ the fitting parameters that depend on the neighbourhood.

$$\mathrm{CV}(\dot{Q}_{\text{arch, SH},\mu}) = a\exp(-b\dot{Q}_{\text{arch, SH},\mu}) + c \tag{4}$$

By stating that the archetype building heat demand is the average building heat demand in a neighbourhood with $N_\mathrm{b}$ buildings and expected heat demand $\dot{Q}_{\mathrm{SH},\mu}$, the following expression for CV can be set up for each neighbourhood:

$$\mathrm{CV}(\dot{Q}_{\mathrm{SH},\mu}) = a\exp(-b\frac{\dot{Q}_{\mathrm{SH},\mu}}{N_\mathrm{b}}) + c \tag{5}$$

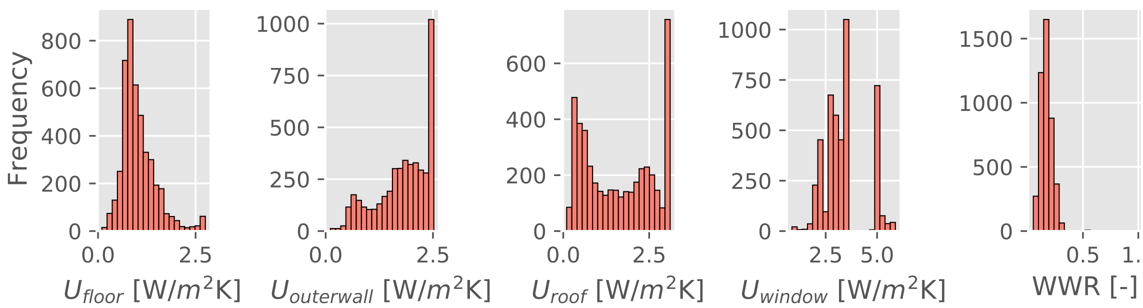


**Figure 3.** Five histograms showing the building parameter distribution in the nine *GenkNET* neighbourhoods, according to the 9x500 variations.

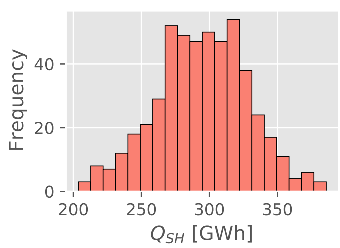


**Figure 4.** A histogram showing the distribution of the annual *GenkNET* heat demand, according to the 500 variations.

In a third part (steps 14-15), the uncertainties (steps 9-13) can be added to the optimal heat demand profiles (steps 5-8). Based on the exponential curves describing the CV, new SH heat demand profiles

[2] The coefficient of variation is the ratio of the standard deviation to the mean of a distribution: $\sigma/\mu$.

for each neighbourhood in *GenkNET* are set up. To do so, a normal distribution is assumed, which has been used in the literature before to describe building heat or electricity demand distributions [23,29,32,38,46]. Considering the distribution in Figure 4, this seems a reasonable assumption. This allows the use of the following quantile function:

$$F^{-1}(p) = \mu + \sigma\sqrt{2}\text{erf}^{-1}(2p-1) \tag{6}$$

For a normally distributed variable, $F^{-1}(p)$ is the value of the variable for which there is a probability $p$ such that $F^{-1}(p)$ is greater than or equal to the variable. In this equation, $\mu$ and $\sigma$ are the expected value and standard deviation of the variable, and $\text{erf}^{-1}$ is the inverse error function.

To set up the SH heat demand profile of version $v$, the following is done. The value for $p$ is randomly selected from a uniform distribution between 0 and 1. Then, starting from the optimal SH heat demand profiles (steps 5-8) [42], at every point in time the quantile function is applied along with the CV that corresponds to the expected heat demand $\dot{Q}_{\text{SH},\mu,\text{i}}$ at the point in time i:

$$\dot{Q}_{\text{SH},v,\text{i}}(p) = \dot{Q}_{\text{SH},\mu,\text{i}}\left(1 + \text{CV}(\dot{Q}_{\text{SH},\mu,\text{i}})\sqrt{2}\text{erf}^{-1}(2p-1)\right) \tag{7}$$

This process yields curves that are scaled by a factor changing through time, with the factor depending on the heat demand at that time.

An additional step is added to introduce a small amount of random behaviour. Following the autoregressive process AR(1), an extra term was added to the heat demand profile. This term has an autocorrelation of 0.75 between two subsequent points in time separated by 15 minutes and it has a standard deviation of 3 % of $\dot{Q}_{\text{SH},\mu,\text{i}}$, following the prediction error analysis in [47].

This way, 100 different SH heat demand profiles are generated for every neighbourhood. To end up with 100 different versions of *GenkNET*, one generated profile of every neighbourhood is grouped together. This grouping was done fully at random, although it could be argued that there might be correlations between neighbourhoods, e.g. if the U-values were underestimated in one neighbourhood, chances are that this happened in other neighbourhoods as well. However, this effect is not included here.

No uncertainty was added to the DHW heat demand, so these are simply added to the different SH heat demand profiles. Finally, the left of Figure 5 shows the heat demand of *GenkNET* of all 100 versions for the *Trans_Negp*$_e$ day. The right graph shows 11 selected profiles, spread over the entire range. Note that the range in variation is similar to that shown in Figure 4, with about a factor 2 between the most extreme cases. The extra random changes that were added to the profile have little effect and do not change the overall behaviour.

### 3.3. Uncertainty analysis

To analyse the influence of heat demand magnitude uncertainty on network flexibility activations, three steps are taken, which are described below.

#### 3.3.1. Step 1: Optimal control of each *GenkNET* version

With 100 possible versions of *GenkNET* created, the optimal control strategy of every version can be calculated. By solving the OCP twice, once with and once without network flexibility, referred to as the Flexibility and Reference cases, the optimal network flexibility activation can be isolated. Six days (see Table 1) will be analysed with respect to operational heat pump optimisation, and peak shaving for different base load ratios (60, 80 and 95 %).

This leads to 100 optimal network flexibility activations for *GenkNET*, based on heat demand profiles that differ mostly in amplitude. This step will show how the optimal control changes as the heat demand magnitude changes.

 

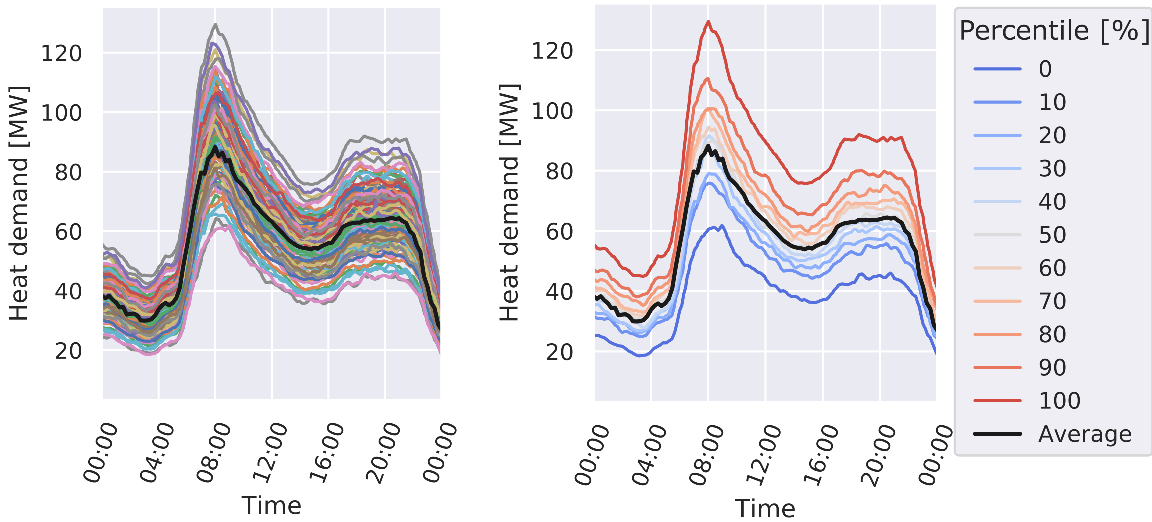


**(a)** All 100 versions. **(b)** 11 evenly spread out versions.

**Figure 5.** The different heat demand profiles of *GenkNET* for the *Trans_Negp$_e$* day. The black line indicates the expected heat demand.

### 3.3.2. Step 2: Selection of 11 control strategies

All *GenkNET* versions are ordered from low to high annual heat demand. Using this ordering, every tenth profile is selected, corresponding to the selection in Figure 5b. Hence, when ordered according to the annual heat demand, versions 0, 10, 20, 30, 40, 50, 60, 70, 80, 90 and 100 are chosen. These versions will be named by these numbers in the remainder of this study, with 0 corresponding to the *GenkNET* version with the lowest annual heat demand and 100 to the one with the highest annual heat demand. Note that the ordering of the profiles is the same for each of the six days and any other variation that is analysed in this study.

### 3.3.3. Step 3: Applying the 11 control strategies to all 100 *GenkNET* versions

Finally, the optimal control strategies of the 11 versions selected in the previous step are applied to all 100 *GenkNET* versions. This leads to 1100 evaluations of *GenkNET* for one day and one optimisation case. This step shows how the optimal control performance changes when the 'predicted' and 'actual' heat demand differ from each other.

## 4. Results

The results are split up into a discussion of the optimisation of heat pump operation and peak shaving optimisation and are presented below.

### *4.1. Operational heat pump optimisation*

The operation of the heat pump is optimised to achieve the lowest possible electricity costs to drive the heat pump while delivering the heat demand to the customers. The electricity prices are based on the 2014 BELPEX day-ahead electricity market.

### 4.1.1. Optimal control of the 11 selected versions

In Step 1 of the uncertainty analysis, the optimal control strategies of all 100 versions of *GenkNET* were calculated. Figure 6 shows the optimal control of the 11 selected versions on the *Winter_Negp$_e$* day (a winter day with an electricity price that becomes negative). These 11 versions are spread out over the entire range of heat demand magnitudes and give a good overview of the optimal control of all versions. Figure 6 shows that the network is charged three times: during the two negative price periods and before a large change in electricity price. With the COP reducing when the supply temperature is increased, which is inevitable when activating network flexibility, these are the only moments when network flexibility is profitable. In Figure 6, the Flexibility and Reference case refer to the cases in which network flexibility is available and in which it is unavailable, respectively.

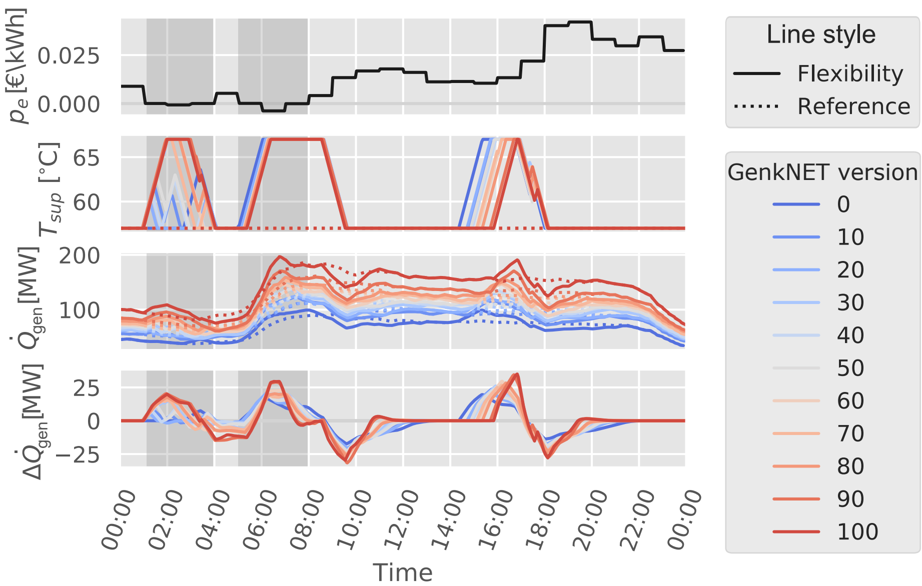


**Figure 6.** For the *Winter_Negp$_e$* day, the results of the operational heat pump optimisation for the 11 selected *GenkNET* versions are shown. From top to bottom, the electricity price, the supply temperature at the plant, the heat injection and the heat injection response (the difference between the Flexibility and Reference case) are shown. The negative price periods are indicated by the dark grey zones.

During the first negative price period, there is a substantial difference between the supply temperature pulses of the different *GenkNET* versions, whereas the pulses are nearly identical in the second negative price period. The differences in the first period are likely caused by the second period that follows shortly after. In the low heat demand versions, the water travels so slowly that charging the network during the first negative period causes the network to discharge during the second, more interesting, negative period, causing a loss in profits. In the high heat demand versions, the water travels faster and the discharge has ended by the time the second negative period starts.

When there is a large price difference, the supply temperature pulse remains similar in all cases but starts earlier as the heat demand reduces, again a consequence of the lower water speeds in the network. Hence, the general actions are largely based on the electricity price profile and remain similar throughout all versions. However, the exact timing can change considerably, with pulse lengths doubling as the heat demand becomes lower. Note that the third pulse always ends at the same point in time, namely when the price increase is taking place.

### 4.1.2. Applying 11 different control strategies to all 100 *GenkNET* versions

In Step 3, the optimal supply temperature profiles in Figure 6 are applied to all 100 versions. This leads to 1100 evaluations for each day, which are presented in Figure 7. Only the three days during which there is a significant network flexibility activation are shown: *Winter_Negp$_e$*, *Trans_Negp$_e$* and *Trans_Large$\Delta p_e$*. For each of the 11 selected control strategies, a box plot is set up. The box plot presents the profit of applying the selected control strategy to all *GenkNET* versions. Studying the median value, it seems that every optimal control strategy achieves a similar profit on average. On the *Trans_Negp$_e$* and *Trans_Large$\Delta p_e$* days, the spread on the profits remains similar as well, regardless of the control strategy. The profits are symmetrically spread around the median and show a possible deviation from the median profit of about 20 % and 33 % on *Trans_Neg*$p_e$ and *Trans_Large*$\Delta p_e$, respectively.

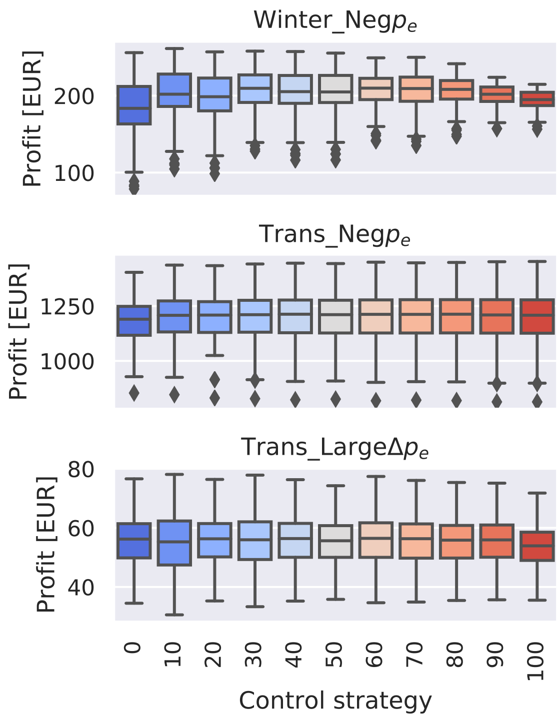


**Figure 7.** Box plots of the profits obtained with the 11 selected control strategies on all *GenkNET* versions for three different days. The box plots shows the median, first and third quartile and the minimum and maximum (excluding outliers) of a data set. The outliers are represented by the diamond markers.

On the *Winter_Neg*$p_e$ day, the profit variation decreases as higher optimal control strategies are applied. Looking back at Figure 6, this is likely caused by the quick succession of two negative price periods. When a higher heat demand is predicted, a large supply temperature pulse is applied during the first negative period. If the actual heat demand is lower, the discharge phase is taking place during the more interesting second negative price period, limiting the profits. Vice versa, if a low heat demand is predicted, but it turns out to be high, the first negative price period was only covered by a small temperature pulse. The spread in profits for control strategies 0 and 100 can be seen in Figure 8, which also shows the difference with the actual optimal solution. It seems that an optimal control strategy based on a different heat demand prediction can lead to a profit reduction by up to a factor 2.

From the cases studied here, it seems that the risk related to heat demand magnitude uncertainty can cause a reduction in profits, yet there was no risk of losing money (negative profits). In general, the control strategy remained similar in all cases, as the control strategy mostly aims for moments with a negative price or with large price changes. The heat demand at those times seems less important.

### *4.2. Peak shaving optimisation*

In the peak shaving optimisation, two plants are available to generate the heat. The base unit can generate heat cheaply but does not have a heat output sufficiently large to deliver the heat demand peaks. The peak unit can cover the peak but at a higher cost. To minimise the cost of heat generation, peak shaving is hence applied by activating network flexibility.

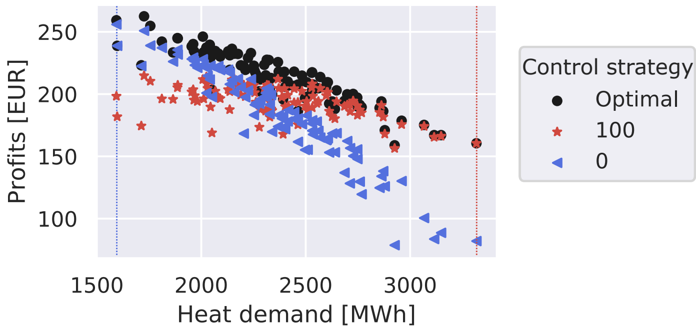


**Figure 8.** On the x-axis the heat demand during the *Winter_Negp*$_e$ day is shown, on the y-axis the profit that was obtained. Every dot represents one version of *GenkNET* managed by one control strategy, the colour and marker shape indicate the applied control strategy. One version will always have the same heat demand, regardless of the applied control strategy. The vertical dotted lines show the heat demand that correspond to the 0 and 100 control strategies.

4.2.1. Optimal control of the 11 selected versions

Figure 9 shows the optimal control results of the 11 selected profiles when the base unit can deliver 95 % of the expected peak heat demand, with a peak-base price ratio of 2 on the *Winter_Large*$\Delta p_e$ day. It shows that the versions with a lower heat demand do not require any network flexibility, while those with a higher heat demand do not succeed in shaving the entire peak. For the versions with the highest heat demand, an additional large supply temperature pulse appears at the end of the peak period. As was explained in [6], a flexibility activation takes place in several phases. First, the network is charged, then it is discharged and at the end a rebound takes place. The rebound compensates the part of the discharge that was not covered by the initial charge. In the last network flexibility activation at the end of the peak period in Figure 9, the initial charge and discharge are both covered by the peak unit, but the rebound is covered by the base unit, effectively moving a small amount of energy from the peak unit to the base unit.

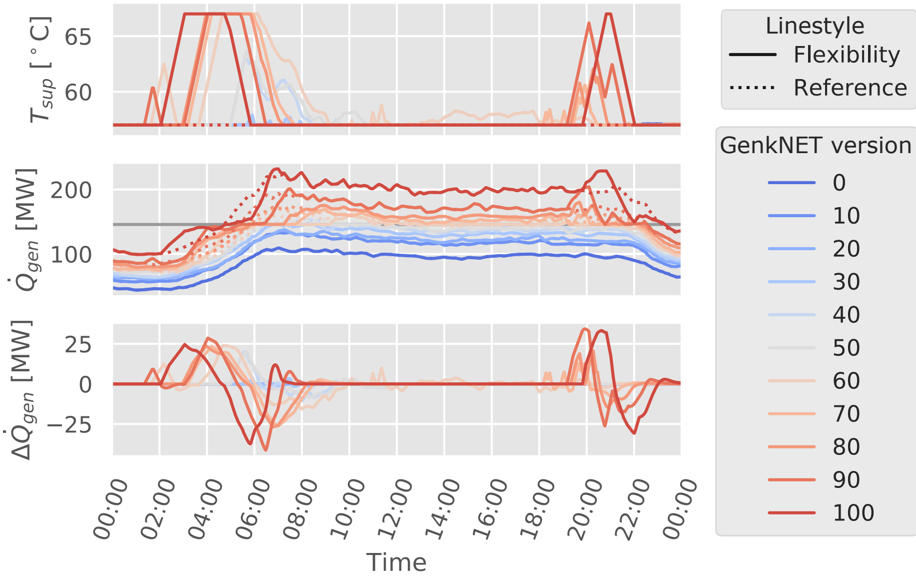


**Figure 9.** For the *Winter_Large*$\Delta p_e$ day, the results of the base-peak plant optimisation for the 11 selected *GenkNET* versions with a base load ratio of 95 % are shown. From top to bottom, the supply temperature at the plant, the heat injection and the heat injection response are shown. In the middle graph, the maximum heat output of the base unit is indicated by the grey horizontal line.

The differences between the different control strategies are clearly larger than for the operational heat pump optimisation. Hence, it is expected that larger ranges of profits (and losses) will appear when applying these strategies to all 100 versions.

#### 4.2.2. Applying 11 different control strategies to all 100 *GenkNET* versions

Figure 10 shows the peak energy that could be avoided in all 100 versions with 11 different control strategies. This is done for the *Winter_Large*$\Delta p_e$ and *Trans_Small*$\Delta p_e$ days for base load ratios of 60, 80 and 95 %. The variation in avoided peak energy has a much larger range than the profit range found for the operational heat pump optimisation. When comparing base load ratios different trends can be observed.

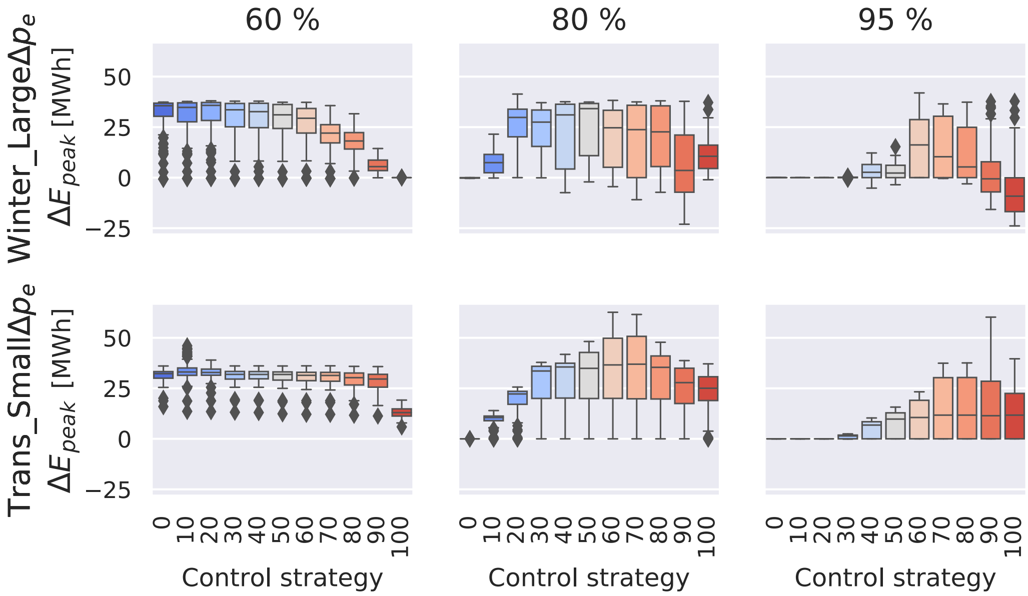


**Figure 10.** Box plots of the avoided peak energy with the 11 selected control strategies on all 100 versions of *GenkNET* for *Winter_Large*$\Delta p_e$ and *Trans_Small*$\Delta p_e$ and for different base load ratios.

Starting on the right of Figure 10 with a base load ratio of 95 %, the lower control strategies cannot accomplish anything at all. Looking back at Figure 9, no network flexibility is required when the heat demand is low, hence there is no network flexibility activation. Going to the higher control strategies, the average peak energy that can be avoided increases as does the possible range, although it always remains mostly positive, i.e. very little to no extra peak energy had to be generated even in the worst case for *Trans_Small*$\Delta p_e$.

However, the highest control strategies on *Winter_Large*$\Delta p_e$ cause extra amounts of peak energy to be generated in many cases. Here, a second large temperature pulse at the end of the peak period has appeared (see Figure 9). This type of network flexibility appears to entail a large risk, as illustrated in Figure 11. If this second pulse is applied to a case with a lower heat demand in which the peak unit is not active at that time, the peak unit might have to be (re)activated to deliver this pulse while the base load is later on reduced, e.g. in version 50. This increases the delivered peak energy substantially. It seems that in case of a large base unit and heat demand magnitude uncertainties, it is better to overestimate than underestimate the heat demand, but to avoid a network flexibility activation at the end of a peak period.

Going to a base load ratio of 80 %, a similar pattern appears, yet everything has shifted to the left; the base unit must now be activated more quickly. The *Winter_Large*$\Delta p_e$ day again shows a risk to generate more peak energy when going to higher control strategies. Again, this is caused by a network flexibility activation at the end of a peak period. This extra pulse has disappeared again at the highest control strategy, which shows no risk to increase the peak energy. The 80 % case shows a clear best

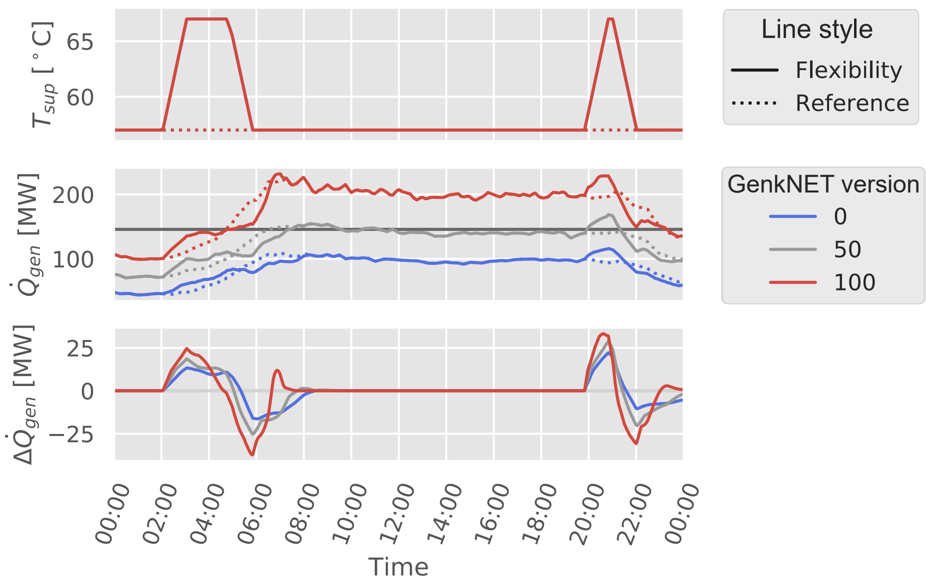


**Figure 11.** The application of control strategy 100 on a *GenkNET* version with low (0), medium (50) and high (100) heat demand on the *Winter_Large*$\Delta p_e$ day with a base load ratio of 95 %. The maximum base unit heat generation is indicated by the horizontal grey line.

result in the intermediate control strategies. For these strategies, the heat demand was high enough that peak shaving is required, but not that high that the peak unit must be active (nearly) all the time, limiting chances for network flexibility.

In case of 60 %, another shift to the left has occurred, the peak unit is now activated even in case of the smallest heat demand. The average avoided peak energy now remains very constant up to the highest control strategies. Here, it decreases again, as hardly any network flexibility is activated any more. The heat demand has now become so high that the base unit must be active (nearly) all the time. Although the range of possible peak energy avoided can be large, there is little risk, i.e. the delivered peak energy will not increase. It seems that in case of a smaller base unit, it would be safe to underestimate the heat demand when deciding a control strategy.

To better understand what occurs when the heat demand changes and what influence the different control strategies have, Figure 12 shows the peak energy that could be avoided for all *GenkNET* cases in six days for a base load ratio of 95 %. For each *GenkNET* version, the result of four different control strategies is shown: the optimal control strategy of that version, the result when the lowest and highest heat demand are 'predicted' and lastly a control strategy that follows the recommendations from before. For a base load ratio of 95 %, it seemed advisable to select a control strategy corresponding to a higher heat demand, without going too high. Hence, control strategy 70 is selected.

The optimal control solutions (black dots) in Figure 12 show some interesting results. With low heat demands, there is no need for peak shaving and hence no peak energy can be avoided either. After a while, the avoided peak starts increasing, until on most days a maximum is reached. This maximum corresponds to the maximum energy storage capacity of the *GenkNET* network (estimated to be 36.8 MWh)[3]. When this maximum is exceeded, there are multiple peaks and network flexibility activations during one day, e.g. a morning and evening peak. These extra peaks appear and disappear as the heat demand magnitude changes.

[3] This number was estimated by calculating the total water mass in the *GenkNET* network, see Figure 2, and multiplying this mass with the specific heat capacity of water and the allowed temperature increase of 10 °C.

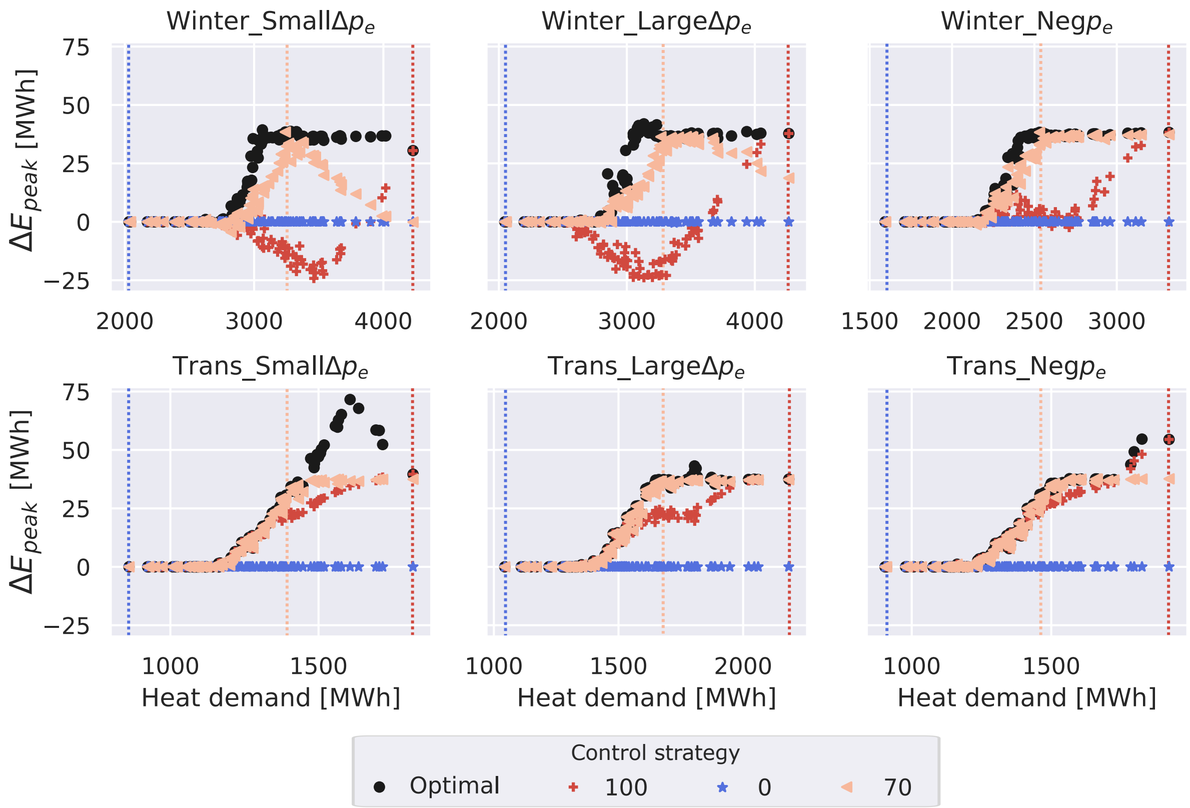


**Figure 12.** On the x-axis the total heat demand during each day and each version is shown, on the y-axis the peak energy that was avoided with a control strategy. Every dot represents one version of *GenkNET* managed by a different control strategy. The vertical dotted lines show the heat demand that correspond to the shown control strategies.

Of all control strategies, the optimal control strategy (black dots) reaches the best result in all cases, as is expected. Control strategy 0 cannot avoid any peak energy, as it does not activate network flexibility. Control strategy 100 can accomplish a reasonable result on the transitional days, noticing the afternoon peak that occurs with the highest heat demands on *Trans_Neg*$p_e$. However, on the winter days, it attempts to activate network flexibility at the end of a peak unit activation, which is risky in case the heat demand turns out to be lower. Lastly, when control strategy 70 is applied, it can in most cases follow the optimal strategy very well. It only misses the afternoon peak of *Trans_Small*$\Delta p_e$ and *Trans_Neg*$p_e$. On *Winter_Small*$\Delta p_e$, its performance decreases with increasing heat demand. Here, the peak period moves significantly through time as the heat demand changes. In case of the highest heat demands, the peak has already started by the time case 70 starts charging the network. This implies that changes in peak timing will complicate the selection of a robust control strategy even further.

Remember that each *GenkNET* version is composed of nine neighbourhoods, of which the heat demand variation was chosen at random and independently of the other neighbourhoods. This means that two *GenkNET* versions with equal total daily heat demand, could have a different distribution of heat demand throughout the nine neighbourhoods and a different reaction to the same supply temperature pulse. Yet, in Figure 12, all points show clear trends. It seems that a different heat demand distribution amongst the *GenkNET* neighbourhoods does not influence the network flexibility activation that much with the currently imposed building parameter distributions.

## 5. Discussion

This study investigates how optimal control changes when the building parameters and hence the heat demand magnitude changes and how the control performance changes when a control strategy based on a different 'predicted' heat demand is applied.

### *5.1. How does the optimal network flexibility activation change when the building parameters/heat demand magnitude changes?*

When the heat demand changes so do the mass flow rates and the network flexibility timing. This is an effect that is visible in the operational heat pump optimisations, although its influence is limited when electricity prices become negative. Only in certain circumstances when multiple negative price periods follow each other shortly, the heat demand magnitude may influence the network flexibility activation to a larger extent.

In case of peak shaving, not only the mass flow rates in the system are important, so is the magnitude of the heat demand with respect to the maximum heat output of the base unit. This can largely influence the network flexibility activation. With a low heat demand, it may be that there is no need for peak shaving, while with a high heat demand network flexibility is not sufficient to shave the entire peak.

### *5.2. How does the network flexibility performance change when the control strategy changes?*

There was relatively little difference in the performance of different control strategies for operational heat pump optimisation.The resulting (average) profits were rather independent of the applied control strategy. Again, in the considered cases it seems that the electricity price timing is at least as important as the heat demand magnitude. Only in special cases (with multiple negative price periods), a significant difference in control strategy performance could be noticed. Hence, for the case of *GenkNET* with variations on building parameters, operational heat pump optimisation does not present much risk. A minimum profit could be guaranteed in all cases.

For peak shaving, another observation can be made. The control strategies were highly dependent on the heat demand magnitude. Yet, an analysis of their performance (i.e. the peak energy that could be shaved) showed that the studied heat demand uncertainty does not introduce much risk. With most control strategies, the generated peak energy remained the same or decreased. In the few cases that network flexibility accomplished a result worse than the Reference case, this was caused by a network flexibility activation at the end of a peak period, or by a large change in the start time of a peak period. This does suggest that uncertainties in timing (related to user behaviour and weather), may induce larger risks.

### *5.3. Does this preliminary study lead to insights for a more robust activation of network flexibility?*

For operational heat pump optimisation, it seems electricity price related uncertainties may be more relevant. Future research should look into this type of uncertainty in more detail to conclude what measures are required to achieve a more robust network flexibility activation. For now, considering only building parameter uncertainties, there seems to be little risk in selecting a control strategy.

For peak shaving, if only heat demand magnitude uncertainties are expected, a recommendation for peak shaving can be made based on the results gathered in this paper. The losses associated with activating network flexibility needlessly are limited, while the possible gains are substantial. Hence, it seems better to activate too much flexibility, instead of too little. Only the activation at the end of a peak period should be avoided as it introduces a risk of generating more peak energy.

### *5.4. Remarks*

This study only considers uncertainties on building parameters. Yet, in reality, these uncertainties may be the least problematic with respect to control. As building parameters do not change, the errors in heat demand predictions caused by them can be corrected over time. By contrast, the user behaviour and weather do change over time and may be much harder to deal with. However, for building parameter data, realistic data distributions could be set up and analysed.

The plant models are simple and do not contain all relevant aspects. For example, the peak unit may require start-up and shut-down costs. These costs increase the risk associated with heat demand uncertainties, as a small peak unit activation may cost much more than was assumed now. Additionally, it was assumed that the base unit can increase the network supply temperature without a reduced efficiency. If the efficiency depends on the supply temperature, this may alter the conclusions made before. Similar things can be said for the heat pump, for ramping limits and costs, etc. A future study should look into these aspects.

The building heat demand profiles were built with small random variations, along with uncorrelated building parameter uncertainties between the neighbourhoods. The results suggest that these aspects have little influence, as the scatter plots of Figures 8 and 12 showed clear trends when ordering the different versions according to the total heat demand during the day. This would indicate that 1) small (random) heat demand variations may not be that important. Hence, predictions may not need to go in great detail, although the extent of this should be investigated. 2) The distribution of the heat demand among the neighbourhoods may not have such a large influence either, although the different neighbourhood locations in the network do influence the network flexibility activation timing. Again, this is another aspect that merits further study.

## 6. Conclusion

This study evaluates the influence of building parameter uncertainties on network flexibility performance. This is done by determining and analysing distributions for building parameters in the city of Genk, Belgium. This led to 100 different profiles describing the heat demand in a fictive DH system in Genk. These heat demand profiles differ mostly in magnitude, not in timing. The optimal control strategy applying network flexibility for these different heat demand profiles was calculated for operational heat pump optimisation and peak shaving. Additionally, control strategies that are optimal for one heat demand profile were applied to all others, to study the influence of an incorrect heat demand prediction.

Analysis of these results shows that building parameter uncertainties do not influence operational heat pump optimisation much, and could reach an average profit that is similar regardless of the applied control strategy. For peak shaving, the heat demand magnitude matters much more, as it is the main factor that determines a peak unit activation. Yet, here the risk remains limited, hence a large network flexibility activation to prevent a possible peak period seems advisable.

**Author Contributions:** Conceptualization, Annelies Vandermeulen, Ina De Jaeger, Tijs Van Oevelen, Dirk Saelens and Lieve Helsen; Data curation, Ina De Jaeger; Formal analysis, Annelies Vandermeulen; Funding acquisition, Annelies Vandermeulen, Ina De Jaeger, Dirk Saelens and Lieve Helsen; Investigation, Annelies Vandermeulen and Ina De Jaeger; Methodology, Annelies Vandermeulen and Ina De Jaeger; Project administration, Dirk Saelens and Lieve Helsen; Software, Annelies Vandermeulen and Ina De Jaeger; Supervision, Tijs Van Oevelen, Dirk Saelens and Lieve Helsen; Validation, Annelies Vandermeulen and Ina De Jaeger; Visualization, Annelies Vandermeulen and Ina De Jaeger; Writing – original draft, Annelies Vandermeulen and Ina De Jaeger; Writing – review & editing, Annelies Vandermeulen, Ina De Jaeger, Tijs Van Oevelen, Dirk Saelens and Lieve Helsen.

**Funding:** This research was funded by VITO grant number 1712 and the FWO-VITO grant number 11D0318N.

**Acknowledgments:** The authors are grateful to Bram van der Heijde for providing the heat demand profiles, as calculated for the GenkNet case study. The work of Annelies Vandermeulen is funded through a PhD Scholarship of the Flemish institute for Technological Research (VITO) (grant number: 1712). Ina De Jaeger holds a PhD grant fundamental research financed by the Research Foundation Flanders (FWO) and the Flemish Institute for Technological Research (VITO) (grant number: 11D0318N).

**Conflicts of Interest:** The authors declare no conflict of interest.

## Abbreviations

The following abbreviations are used in this manuscript:

| | |
|---|---|
| CHP | Combined Heat and Power |
| CV | Coefficient of Variation |
| DH | District Heating |
| DHC | District Heating and Cooling |
| DHW | Domestic Hot Water |
| LDC | Load Duration Curve |
| MPC | Model Predictive Control |
| OCP | Optimal Control Problem |
| $R^2ES$ | Renewable and Residual Energy Sources |
| SH | Space Heating |
| TES | Thermal Energy Storage |

## Appendix A. Optimal control component models and settings

This appendix shortly presents the component models included in the OCP solved in this paper, along with the optimisation settings. For a more detailed overview of the applied optimal control problem, please refer to [48].

### *Appendix A.1. Pipe model*

The pipe model is an explicit transient first-order upwind finite volume model, as has been used before in the literature [49–56]. The energy balance of one finite volume is described in Equation A1. $m_\mathrm{k}$ is the mass of water in one finite volume, $c_\mathrm{p}$ is the specific heat capacity of water, $i$ and $k$ are indices indicating the time step and the finite volume, respectively. $T_\mathrm{i,k}$ is the temperature of one finite volume at one instance in time, $\Delta t$ is the length of the time step, $\dot{m}$ is the mass flow rate through the pipe, $T_\mathrm{g}$ is the ground temperature and $R$ is the thermal resistance between water and surrounding ground.

$$m_\mathrm{k} c_\mathrm{p} (T_\mathrm{i,\,k} - T_\mathrm{i\text{-}1,\,k}) + \dot{m}_\mathrm{i} c_\mathrm{p} \Delta t (T_\mathrm{i\text{-}1,\,k} - T_\mathrm{i\text{-}1,\,k\text{-}1}) = \frac{T_\mathrm{g} - T_\mathrm{i\text{-}1,\,k}}{R} \Delta t \tag{A1}$$

To account for the wall thermal inertia, a correction at the end of a pipe has been added. This correction is given in Equation A2 and follows the technique presented by Benonysson [57]. Here, $T'_\mathrm{out,\,i}$ is the temperature exiting the pipe corrected for the wall thermal inertia, while $T_\mathrm{out,\,i}$ is the temperature exiting the pipe as calculated by the finite volume model. $C_\mathrm{pipe}$ is the thermal capacity of of the pipe wall, $T_\mathrm{wall,\,k}$ is the pipe wall temperature. The wall temperature is updated through time by Equation A3

$$T'_\mathrm{out,\,i} = \frac{T_\mathrm{out,\,i} \dot{m}_\mathrm{i} c_\mathrm{p} \Delta t + C_\mathrm{pipe} T_\mathrm{wall,\,i\text{-}1}}{C_\mathrm{pipe} + \dot{m}_\mathrm{i} c_\mathrm{p} \Delta t} \tag{A2}$$

$$T_\mathrm{wall,\,i} = T'_\mathrm{out,\,i} \tag{A3}$$

This finite volume model is only stable if the following condition related to the spatial and temporal discretisation is met:

$$\mathrm{CFL} = \frac{u \Delta t}{\Delta x} \leq 1 \tag{A4}$$

In this equation, $u$ is the speed of water through the pipe and $\Delta x$ is axial length of a finite volume. The closer CFL is to one, the less numerical diffusion takes place and the more accurate the model is. Similarly, the finer the discretisation is, i.e. the smaller $\Delta x$ and $\Delta t$ are, the more accurate the model is. However, a finer discretisation causes a quadratic increase in calculation time. To discretise, a careful selection of the spatial discretisation ($\Delta x$) and temporal discretisation ($\Delta t$) were made such that the accuracy is sufficiently high and the problem remains solvable within an acceptable time. The model accuracy was tested by comparing it to Modelica simulations of both a validated pipe model [58] and a *GenkNET* DH system model consisting of detailed component models. For more information, please refer to [48].

### Appendix A.2. Substation model

The substation model that is included in the OCP is the *No HEx* model derived and described in [6]. This model is based on a substation with two heat exchangers, one for space heating (with radiator heating) and one for domestic hot water (DHW). Although the building heating system and the heat exchangers are modelled, the heat demand profiles are determined in advance [42], hence no building structure model is included. The *No HEx* model is a simplified version of the original detailed substation model. *No HEx* only includes a 2D look-up table that gives the primary return temperature exiting the substation in function of the space heating and DHW heat demand and the incoming primary supply temperature.

Again, this model was tested and verified by comparing it with simulation of a *GenkNET* DH system model consisting of detailed component models.

### Appendix A.3. Heat pump model

The *GenkNET* central heat pump is an electric air-to-water heat pump. An important parameter is the coefficient of performance (COP). This is the ratio of $\dot{Q}_{\text{gen}}$ the heat supplied to the DH system to $\dot{W}$ the electrical power required.

$$\text{COP} = \frac{\dot{Q}_{\text{gen}}}{\dot{W}} \tag{A5}$$

Representing a heat pump by a Carnot cycle, the COP can be expressed as a function of the condenser and evaporator temperatures, corresponding to $T_{\text{gen, sup}}$ and $T_{\text{e}}$, the DH supply and ambient air temperatures, respectively. As real heat pumps do not follow the ideal Carnot cycle, an additional efficiency $\eta_C$ is introduced, taking the value of 0.6 [42]. $\eta_C$ incorporates the efficiency loss due to non-adiabatic compression, isenthalpic expansion, non-isothermal heat exchange, etc. The air temperature $T_{\text{e}}$ corresponds to the typical meteorological year in Uccle (BE).

$$\text{COP} = \eta_C \frac{T_{\text{gen, sup}}}{T_{\text{gen,sup}} - T_{\text{e}}} \tag{A6}$$

The plant then delivers heat to the DH system, according to Equation A7, with $\dot{m}_{\text{gen}}$, $T_{\text{gen,sup}}$ and $T_{\text{gen, ret}}$ the DH mass flow rate, supply and return temperatures at the plant, respectively.

$$\dot{Q}_{\text{gen}} = \dot{m}_{\text{gen}} c_{\text{p}} (T_{\text{gen,sup}} - T_{\text{gen, ret}}) \tag{A7}$$

The following constraint to limit temperature ramping is added:

$$\frac{-10\,^{\circ}\text{C}}{3600\,\text{s}} \Delta t \leq T_{\text{gen,sup, i}} - T_{\text{gen, sup, i-1}} \leq \frac{-10\,^{\circ}\text{C}}{3600\,\text{s}} \Delta t \tag{A8}$$

This equation limits the supply temperature changes between two points in time (i and i-1), separated by $\Delta t$ seconds in accordance with EN 13941 [59]. Additionally, the supply temperature can only change between the nominal value $T_{\text{sup, nom}}$ and a temperature that is 10 °C higher, giving it the required degree of freedom to activate network flexibility:

$$T_{\text{sup, nom}} \leq T_{\text{gen, sup}} \leq T_{\text{sup, nom}} + 10\,^{\circ}\text{C} \tag{A9}$$

The heat output is only constrained to be positive, as in Equation A10. There is no maximum value the heat output can take, nor any limit on how fast the heat output can increase. However, with the temperature ramping constraint in place and the *GenkNET* heat demand profiles determined in advance, the values the plant heat output can take will at all times be acceptable.

$$0 \leq \dot{Q}_{\text{gen}} \tag{A10}$$

*Appendix A.4. Base and peak plant model*

In a second possible heat generation site, a base and peak plant work together. The base plant is cheap, but has a maximum heat output that is insufficient to deliver all heat demand. The peak plant is more expensive, but can supplement the base heat output to deliver all heat demand. In this case peak shaving could reduce operational costs.

The base and peak plant are modelled as follows:

$$\dot{Q}_{\text{gen}} = \dot{Q}_{\text{b}} + \dot{Q}_{\text{p}} = \dot{m}_{\text{gen}} c_{\text{p}} (T_{\text{gen, sup}} - T_{\text{gen, ret}}) \tag{A11}$$

with $\dot{Q}_{\text{gen}}$ the total heat generated by both base and peak plant and $\dot{Q}_{\text{b}}$ and $\dot{Q}_{\text{p}}$ is the heat generated by the base and peak unit separately.

Along with the constraints in Equations A8 and A9, the following limits on heat output are also included:

$$0 \leq \dot{Q}_{\text{b}} \leq \dot{Q}_{\text{b, max}} \tag{A12}$$

$$0 \leq \dot{Q}_{\text{p}} \tag{A13}$$

The base plant heat output is limited by $\dot{Q}_{\text{b, max}}$. The peak plant, just like the heat pump, does not have any limit on the maximum power output. Again, the heat output will be limited due to the pre-defined heat demand profiles and supply temperature constraints.

*Appendix A.5. Optimal control model settings*

The horizon of the optimisation problem is 24 hours, with a time step that changes through time, but is always smaller than 5 minutes. Each pipe in the network contains at least 3 and at most 22 finite volumes. These measures keep the CFL-number as close to 1 as possible and the problem size as limited as possible. The combination of all component models previously presented with mass and energy balances, leads to a non-linear program that is solved in `modesto` [39] with `ipopt` [60].

## References


1. European Commission. Statistical office of the European Union.; 2019.
2. Fleiter, T.; Steinbach, J.; Ragwitz, M. Mapping and Analysis of the Current and Future (2020-2030) heating/cooling fuel deployment (fossils/renewables) **September 2016**.
3. European Commission. An EU Strategy on Heating and Cooling, 2016.
4. Frederiksen, S.; Werner, S. *District Heating and Cooling*; Studentlitteratur, 2014.
5. Connolly, D.; Lund, H.; Mathiesen, B.V.; Werner, S.; Möller, B.; Persson, U.; Boermans, T.; Trier, D.; Østergaard, P.A.; Nielsen, S. Heat Roadmap Europe : Combining district heating with heat savings to decarbonise the EU energy system. *Energy Policy* **2014**, *65*, 475–489. doi:10.1016/j.enpol.2013.10.035.
6. Vandermeulen, A.; Van Oevelen, T.; van der Heijde, B.; Helsen, L. A simulation-based evaluation of substation models for network flexibility characterisation in district heating networks. *Energy* **2020**, p. 117650. doi:https://doi.org/10.1016/j.energy.2020.117650.
7. Vandermeulen, A.; van der Heijde, B.; Helsen, L. Controlling district heating and cooling networks to unlock flexibility: A review. *Energy* **2018**, *151*, 103–115. doi:10.1016/j.energy.2018.03.034.
8. Giraud, L.; Merabet, M.; Baviere, R.; Vallée, M. Optimal Control of District Heating Systems using Dynamic Simulation and Mixed Integer Linear Programming. Proceedings of the 12th International Modelica Conference; , 2017; pp. 141–150. doi:10.3384/ecp17132141.
9. Bavière, R.; Vallée, M. Optimal Temperature Control of Large Scale District Heating Networks. *Energy Procedia* **2018**, *149*, 69–78. doi:10.1016/j.egypro.2018.08.170.

10. Ikonen, E.; Selek, I.; Kovacs, J.; Neuvonen, M.; Szabo, Z.; Bene, J.; Peurasaari, J. Short term optimization of district heating network supply temperatures. ENERGYCON 2014 - IEEE International Energy Conference; , 2014; pp. 996–1003. doi:10.1109/ENERGYCON.2014.6850547.
11. Benonysson, A.; Bøhm, B.; Ravn, H.F. Operational optimization in a district heating system. *Energy Conversion and Management* **1995**, *36*, 297–314. doi:https://doi.org/10.1016/0196-8904(95)98895-T.
12. Laakkonen, L.; Korpela, T.; Kaivosoja, J.; Vilkko, M.; Majanne, Y.; Nurmoranta, M. Predictive Supply Temperature Optimization of District Heating Networks Using Delay Distributions. *Energy Procedia* **2017**, *116*, 297–309. doi:10.1016/j.egypro.2017.05.076.
13. Leśko, M.; Bujalski, W.; Futyma, K. Operational optimization in district heating systems with the use of thermal energy storage. *Energy* **2018**, *165*, 902–915. doi:10.1016/j.energy.2018.09.141.
14. Dominković, D.F.; Junker, R.G.; Lindberg, K.B.; Madsen, H. Implementing flexibility into energy planning models: Soft-linking of a high-level energy planning model and a short-term operational model. *Applied Energy* **February 2020**, *260*, 114292. doi:10.1016/j.apenergy.2019.114292.
15. Gu, W.; Wang, J.; Lu, S.; Luo, Z.; Wu, C. Optimal operation for integrated energy system considering thermal inertia of district heating network and buildings. *Applied Energy* **2017**, *199*, 234–246. doi:10.1016/j.apenergy.2017.05.004.
16. Li, Z.; Wu, W.; Shahidehpour, M. Combined Heat and Power Dispatch Considering Pipeline Energy Storage of District Heating Network. *IEEE Transactions on Sustainable Energy* **2016**, *7*, 12–22.
17. Tian, L.; Xie, Y.; Hu, B.; Liu, X.; Deng, T.; Luo, H.; Li, F. A Deep Peak Regulation Auxiliary Service Bidding Strategy for CHP Units Based on a Risk-Averse Model and District Heating Network Energy Storage. *Energies* **2019**, *12*, 1–27.
18. Kim, S.H. An evaluation of robust controls for passive building thermal mass and mechanical thermal energy storage under uncertainty. *Applied Energy* **2013**, *111*, 602–623. doi:10.1016/j.apenergy.2013.05.030.
19. Baetens, R.; Saelens, D. Modelling uncertainty in district energy simulations by stochastic residential occupant behaviour. *Journal of Building Performance Simulation* **September 2015**, *1493*, 1–17. doi:10.1080/19401493.2015.1070203.
20. Strathclyde University. Demand Profile Genrator.
21. Rysanek, A.M.; Choudhary, R. DELORES – an open-source tool for stochastic prediction of occupant services demand. *Journal of Building Performance Simulation* **2015**, *8*, 97–118. doi:10.1080/19401493.2014.888595.
22. Yamaguchi, Y.; Kambayashi, Y.; Okada, T.; Shoda, Y.; Shimoda, Y. Community-Scale Household Activity Modelling Considering Household Heterogeneity Using Japanese Time Use Data. Proceedings of the Urban Energy Simulation Conference; , 2017; pp. 1–6.
23. Oldewurtel, F. Stochastic Model Predictive Control for Energy Efficient Building Climate Control. Phd thesis, PhD thesis, ETH Zurich, 2011.
24. Reinhart, C.F.; Cerezo Davila, C. Urban building energy modeling – A review of a nascent field. *Building and Environment* **2016**, *97*, 196–202. doi:10.1016/j.buildenv.2015.12.001.
25. Kavgic, M.; Mavrogianni, A.; Mumovic, D.; Summerfield, A.; Stevanovic, Z.; Djurovic-Petrovic, M. A review of bottom-up building stock models for energy consumption in the residential sector. *Building and Environment* **2010**, *45*, 1683–1697, [arXiv:1011.1669v3]. doi:10.1016/j.buildenv.2010.01.021.
26. Cuypers, D.; Vandevelde, B.; Van Holm, M.; Verbeke, S. Belgische woningtypologie: nationale brochure over de TABULA woningtypologie. Technical report, 2014.
27. De Coninck, R.; Helsen, L. Practical implementation and evaluation of model predictive control for an office building in Brussels. *Energy and Buildings* **2016**, *111*, 290–298. doi:10.1016/j.enbuild.2015.11.014.
28. Arnold, M.; Andersson, G. Model Predictive Control of Energy Storage including Uncertain Forecasts. Power Systems Computation Conference (PSCC); , 2011; pp. 24–29.
29. Bruninx, K.; Patteeuw, D.; Delarue, E.; Helsen, L.; D'Haeseleer, W. Short-term demand response of flexible electric heating systems: The need for integrated simulations. International Conference on the European Energy Market, EEM; IEEE: Stockholm, Sweden, 2013; Number May, pp. 28–30. doi:10.1109/EEM.2013.6607333.
30. Verrilli, F.; Parisio, A.; Glielmo, L. Stochastic Model Predictive Control for Optimal Energy Management of District Heating Power Plants. 2016 IEEE 55th Conference on Decision and Control; , 2016; Number Cdc.

31. Wang, C.; Jiao, B.; Guo, L.; Tian, Z.; Niu, J.; Li, S. Robust scheduling of building energy system under uncertainty. *Applied Energy* **2016**, *167*, 366–376. doi:10.1016/j.apenergy.2015.09.070.
32. Gao, D.c.; Sun, Y.; Lu, Y. A robust demand response control of commercial buildings for smart grid under load prediction uncertainty. *Energy* **2015**, *93*, 275–283. doi:10.1016/j.energy.2015.09.062.
33. Rosenblueth, E. Point estimates for probability moments. Proceedings of the National Academy of Sciences, 1975, Vol. 72, pp. 3812–3814.
34. Massrur, H.R.; Niknam, T.; Fotuhi-Firuzabad, M. Investigation of Carrier Demand Response Uncertainty on Energy Flow of Renewable-Based Integrated Electricity-Gas-Heat Systems. *IEEE Transactions on Industrial Informatics* **2018**, *14*, 5133–5142. doi:10.1109/TII.2018.2798820.
35. Kitapbayev, Y.; Moriarty, J.; Mancarella, P. Stochastic control and real options valuation of thermal storage-enabled demand response from flexible district energy systems. *Applied Energy* **2015**, *137*, 823–831. doi:10.1016/j.apenergy.2014.07.019.
36. Diehl, M.; Gerhard, J.; Marquardt, W.; Mönnigmann, M. Numerical solution approaches for robust nonlinear optimal control problems. *Computers and Chemical Engineering* **2008**, *32*, 1279–1292. doi:10.1016/j.compchemeng.2007.06.002.
37. Lin, J.G.G. On min-norm and min-max methods of multi-objective optimization. *Mathematical Programming* **2005**, *103*, 1–33. doi:10.1007/s10107-003-0462-y.
38. Rantzer, J. Robust Production Planning for District Heating Networks. PhD thesis, Master thesis, Lund University, Sweden, 2015.
39. Vandermeulen, A.; van der Heijde, B.; Vanhoudt, D.; Salenbien, R.; Helsen, L. modesto - a Multi-Objective District Energy Systems Toolbox for Optimisation. Solar District Heating Conference; , 2018.
40. Wang, H.; Lahdelma, R.; Wang, X.; Jiao, W.; Zhu, C.; Zou, P. Analysis of the location for peak heating in CHP based combined district heating systems. *Applied Thermal Engineering* **2015**, *87*, 402–411. doi:10.1016/j.applthermaleng.2015.05.017.
41. Vandermeulen, A.; Reynders, G.; van der Heijde, B.; Vanhoudt, D.; Salenbien, R.; Saelens, D.; Helsen, L. Sources of energy flexibility in district heating networks: building thermal inertia versus thermal energy storage in the network. Proceedings of Urban Energy Simulations Conference; , 2018.
42. van der Heijde, B.; Vandermeulen, A.; Salenbien, R.; Helsen, L. Integrated Optimal Design and Control of Fourth Generation District Heating Networks with Thermal Energy Storage. *Energies* **2019**, *12*, 2766. doi:10.3390/en12142766.
43. Remmen, P.; Lauster, M.; Mans, M.; Fuchs, M.; Osterhage, T.; Müller, D. TEASER: an open tool for urban energy modelling of building stocks. *Journal of Building Performance Simulation* **2018**, *11*, 84–98. doi:10.1080/19401493.2017.1283539.
44. De Jaeger, I.; Reynders, G.; Ma, Y.; Saelens, D. Impact of building geometry description within district energy simulations. *Energy* **2018**, *158*, 1060–1069. doi:10.1016/j.energy.2018.06.098.
45. Baetens, R.; De Coninck, R.; Jorissen, F.; Picard, D.; Helsen, L.; Saelens, D. OpenIDEAS – an Open Framework for Integrated District Energy Simulations. BS2015, 14th Conference of International Building Performance Simulation Association; , 2015; pp. 347–354.
46. Serrano-Guerrero, X.; Escrivá-Escrivá, G.; Roldán-Blay, C. Statistical methodology to assess changes in the electrical consumption profile of buildings. *Energy and Buildings* **2018**, *164*, 99–108. doi:10.1016/j.enbuild.2017.12.059.
47. Bünning, F.; Heer, P.; Smith, R.S.; Lygeros, J. Improved day ahead heating demand forecasting by online correction methods. *Energy & Buildings* **2020**, *211*. doi:10.1016/j.enbuild.2020.109821.
48. Vandermeulen, A. Quantification and optimal control of network flexibility in district heating systems. PhD Thesis, under evaluation, KU Leuven, Belgium, 2020.
49. Guelpa, E.; Sciacovelli, A.; Verda, V. Thermo-fluid dynamic model of large district heating networks for the analysis of primary energy savings. *Energy* **2019**, *184*, 34–44. doi:10.1016/j.energy.2017.07.177.
50. Kudela, L.; Chylek, R.; Pospisil, J. Performant and simple numerical modeling of district heating pipes with heat accumulation. *Energies* **2019**, *12*. doi:10.3390/en12040633.
51. Betancourt Schwarz, M.; Mabrouk, M.T.; Santo Silva, C.; Haurant, P.; Lacarrière, B. Modified finite volumes method for the simulation of dynamic district heating networks. *Energy* **2019**, *182*, 954–964. doi:10.1016/j.energy.2019.06.038.

52. Borsche, R.; Eimer, M.; Siedow, N. A local time stepping method for thermal energy transport in district heating networks. *Applied Mathematics and Computation* **2019**, *353*, 215–229. doi:10.1016/j.amc.2019.01.072.
53. Rein, M.; Mohring, J.; Damm, T.; Klar, A. Optimal control of district heating networks using a reduced order model. *arXiv preprint arXiv:1907.05255* **2019**.
54. Sartor, K.; Thomas, D.; Dewallef, P. A comparative study for simulating heat transport in large district heating networks. *International Journal of Heat and Technology* **2018**, *36*, 301–308.
55. Wang, Y.; You, S.; Zhang, H.; Zheng, X.; Zheng, W.; Miao, Q.; Lu, G. Thermal transient prediction of district heating pipeline: Optimal selection of the time and spatial steps for fast and accurate calculation. *Applied Energy* **August 2017**, *206*, 900–910. doi:10.1016/j.apenergy.2017.08.061.
56. Vivian, J.; Monsalvete Alvarez de Uribarri, P.; Eicker, U.; Zarrella, A. The effect of discretization on the accuracy of two district heating network models based on finite-difference methods. 16th International Symposium on District Heating an Cooling; , 2018; pp. 1–10.
57. Bennonysson, A. Dynamic Modelling and Operation Optimization of District Heating Systems. Doctoral thesis, Technical University of Denmark, Denmark, 1991.
58. van der Heijde, B.; Fuchs, M.; Ribas Tugores, C.; Schweiger, G.; Sartor, K.; Basciotti, D.; Müller, D.; Nytsch-geusen, C.; Wetter, M.; Helsen, L. Dynamic equation-based thermo-hydraulic pipe model for district heating and cooling systems. *Energy Conversion and Management* **2017**, *151*, 158–169. doi:10.1016/j.enconman.2017.08.072.
59. European Standard. *EN 13941:2019 District heating pipes. Design and installation of thermal insulated bonded single and twin pipe systems for directly buried hot water networks.*
60. Wächter, A.; Biegler, L.T. On the implementation of an interior-point filter line-search algorithm for large-scale nonlinear programming. *Mathematical Programming* **2006**, *106*, 25–57. doi:10.1007/s10107-004-0559-y.